IEEE Access
Multidisciplinary | Rapid Review | Open Access Journal

Received March 15, 2021, accepted March 19, 2021, date of publication March 23, 2021, date of current version April 6, 2021.

Digital Object Identifier 10.1109/ACCESS.2021.3068338

VHF/UHF Miniaturized Ferrite-EBG Composited Choke Structures

DONGJIE QIN AND BAOHUA SUN
National Key Laboratory of Antennas and Microwave Technology, Xidian University, Xi'an 710071, China
Corresponding author: Baohua Sun (bhsun@mail.xidian.edu.cn)

ABSTRACT Parasitic currents on the sheaths of the coaxial cables will deteriorate the performance of the antenna, so the choke structures are needed. While a-quarter-wavelength choke sheaths at VHF and UHF are very long, miniaturized ferrite-EBG composited choke structures are proposed. The ferrite refers to ferrite magnetic beads. Electromagnetic bandgap (EBG) element is consisted of multi-section metal tubes with length relatively shorter than a-quarter-wavelength. The integrated structures are formed by arranging EBG elements and beads alternately along the coaxial line. The proposed choke structures combine the wideband choke performance of the ferrite beads and the high efficiency of the EBG structures. Furthermore, due to the difficulty of the quantitative measurement of the choke structures in an open space, a measuring setup designed in a transmission line model is devised. The choking effects of the proposed structures can be characterized by the $|S_{21}|$ parameter of the measuring device, as the direction of the currents flowing on the sheaths of feeding cables are the same as that of the currents on the inner conductor of the measuring device. Meanwhile, choking bandwidth, efficiency and size of the ferrite-EBG composited choke structures are compared with that of EBG structures and beads. The influence of different numbers of the proposed structures is studied. A prototype is fabricated and measured. The overall size of the ferrite-EBG composited choke structures is $0.25\ \lambda_L \times 0.024\ \lambda_L \times 0.024\ \lambda_L$ (415 mm × 40 mm × 40 mm) (λ_L is the wavelength of the lower end of the operating frequency band). The measured choking band ($|S_{21}| < -10$ dB) is in the region of 181-343 MHz.

INDEX TERMS Balun, beads, choke, EBG, monopole, VHF, UHF.

I. INTRODUCTION

Flowing parasitic currents on the sheaths of the feeding coaxial lines that are caused by unbalanced feed will deteriorate the performance of the antennas, such as making the input impedance unmatched, deforming the radiation patterns, and lowering the gain. Furthermore, the unwanted currents will lower the efficiency of the whole communication system. Choke structures are applied to address this problem, [1], [2], [4] and [9].

For vehicle-mounted monopole or dipole antennas at very high frequency (VHF) band and ultrahigh frequency (UHF) band, common choke structures, such as a-quarter-wavelength choke sheaths, are of long length. Take 30 MHz for instance, the choke sheath is 2.5 meters long at this frequency that is not suitable for the vehicle application. The miniaturization of the choke structures is a crucial problem. But relevant research and documents at this frequency region are rare and not up-to-date, for example [1], [4] and [9].

Choke structures can be generally classified into two types in terms of the designing process: one is designed with antenna together that serves the specific antenna, and the other is designed separately with antennas, which can be generally used in different antennas [1]–[3]. This paper belongs to the latter.

Choke structures have been applied in following situations: suppressing the currents flowing along the feeding lines in [1]–[13], reducing the mutual coupling between two adjacent antennas by attenuating the currents flowing on the sharing ground in [1], [10], and [14], realizing effective utilization of the antenna aperture, and mitigating the low-angle multipath electromagnetic interference in the positioning antenna in [20]–[24]. Choke structures of several types for different antennas, such as whip antennas and patch antennas, are reported by researchers in many papers. Choke structures are generally summarized in three categories: ferrite beads,

The associate editor coordinating the review of this manuscript and approving it for publication was Guangcun Shan.

a-quarter-wavelength choke sleeves, and LC resonating circuits with lumped elements, distributed structures, or the composition of them.

Ferrite beads are the common and very effective method used on coaxial lines [4] and in actual antennas [5] to choke the parasitic currents, which have good choking performance and relatively broad choke band from several MHz to several hundred MHz. However, the efficiency of the ferrite beads is usually low. With frequency increasing, the permeability of the ferrite material drops dramatically, so the parasitic currents on the cables are not blocked based on the principle of magnetic fields effect, but turn into heat on the beads, which brings a problem of heat dissipation [25].

A-quarter-wavelength choke sleeves are mostly used as choke structures due to their excellent choking performance and can be used in different operating frequency without the restriction as ferrite beads. Many papers report this structures, such as a-quarter-wavelength choke sleeves in tube antennas or cable sheaths in [6]–[8], and [17], a-quarter-wavelength slot in [11], [12], [16], and [18] or meandered lines in patch antennas in [13], or a set of concentric a-quarter-wavelength-deep choke rings in [20]–[24]. But they can only operate at a relatively narrow frequency band. To widen the bandwidth, a novel structure, composed by arranging several a-quarter-wavelength sleeves which operate at different frequency points along the feeding line to realize a wide choking band, is proposed in [1], but the length is too long (710 mm).

LC resonating circuits, just acting as band-stop filters that operate at the frequency of the parasitic currents, are the new methods to solve the problem, which are usually composed of lumped or distributed inductors and capacitors. Metal poles and rings are exploited in [2] to form a resonating circuit for blocking currents. Designed on the coaxial lines in [3] and [9], the choke structures are formed with several series of resonating circuits. Resonating circuits are composed of slots or metal lines on printed circuit boards in [10], [14] and [15] to choke the unwanted currents. Electromagnetic bandgap (EBG) structures in [19] can be interpreted to periodic series of distributed LC resonating circuits in essence, employing the periodicity of metal structures to suppress the parasitic currents propagating along the metal structure.

Miniaturized ferrite-EBG composited choke structures, composed of EBG structures and ferrite magnetic beads, are proposed in this paper, seen as Fig. 1. The ferrite refers to the ferrite magnetic beads. The EBG structures are consisted of multi-section aluminum tubes, and the length of the EBG element is relatively shorter than a quarter wavelength. With beads inside the EBG structures, the integrated structures are formed by arranging EBG elements and beads alternately along the sheath of the feeding coaxial line. The beads used in this design are to improve the equivalent inductance of the choke structures, instead of utilizing the loss of the beads to choke currents. Meanwhile, the EBG structures serve as the cooling shells for the beads which solve the heat dissipation of the beads at high frequencies [25]. The proposed

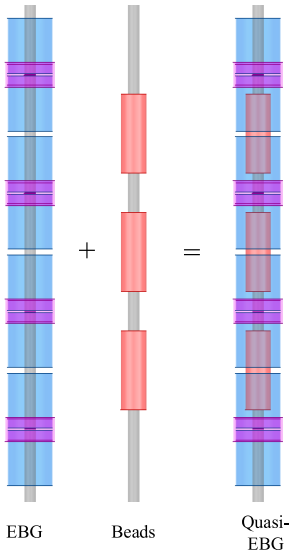

FIGURE 1. The design concept of the ferrite-EBG choke structures.

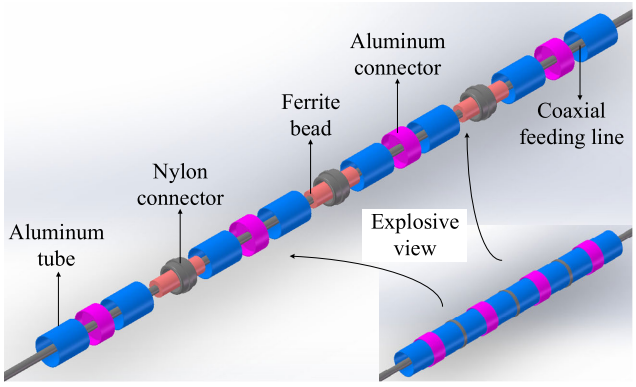

FIGURE 2. The assembly of the ferrite-EBG choke structures.

model combines the merits of both the wideband choking performance of the ferrite beads and the high efficiency of the EBG structures. This paper is organized as follows: Section II presents the design details of the ferrite-EBG composited choke structures and the operating principle. The measuring device is introduced in Section III. Section IV shows the performance and the investigation of the ferrite-EBG choke structures. The fabricated prototype and the measuring results are presented in Section V. Finally, section VI gives a concise conclusion.

II. CHOKE STRUCTURES AND OPERATING PRINCIPLE

A. THE DESIGN DETAILS OF THE CHOKE STRUCTURES

As shown in Fig. 1, the design concept is compositing the EBG structures and the beads together, and combines the advantages of the both structures, which provides a compromise choice between the bandwidth and the efficiency. For easy installation, the ferrite-EBG composited choke structures are designed in separated components, with the explosive assembly view shown in Fig. 2. The EBG element has two aluminum tubes (shown in Fig. 3 (a)) connected by an

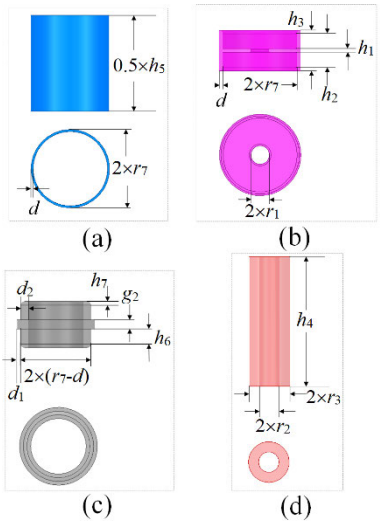

FIGURE 3. Three views and specific dimensions of the elements of the ferrite-EBG structures. (a) Aluminum tube. (b) Aluminum connector. (c) Nylon connector. (d) Bead.

TABLE 1. Parameters of the beads.

Parameters	Value
material	Ni-Zn
initial permeability	16±3.2
ratio loss coefficient	32000(700 MHz)
temperature coefficient	3000(+25°C~+85°C)
resistivity	$10^5 \Omega m$
maximum operating frequency	700 MHz
external diameter × *internal diameter* × *height*	22 mm×11 mm ×10 mm

TABLE 2. Parameters of the Ferrite-EBG structures (Unit: mm).

Variables	Value	Variables	Value
r_1	5	h_1	2
r_2	5.5	h_2	18
r_3	11	h_3	22
r_7	20	h_4	70
d	1	h_5	100
d_1	2	h_6	8
d_2	4	h_7	2
g_2	5		

aluminum connector (shown in Fig. 3 (b)), and the EBG element is connected with the outer conductor of the coaxial line through the middle hole. The nylon connector, shown in Fig. 3 (c), is designed to keep the fixed distance between two EBG elements. The bead element is shown in Fig. 3 (d), and the detail information is shown in Table 1. The specific dimensions are marked with variables in Fig. 3, and the variables are listed in Table 2. Four important variables (g_2, h_4, h_5, and r_7) are studied in the section IV.

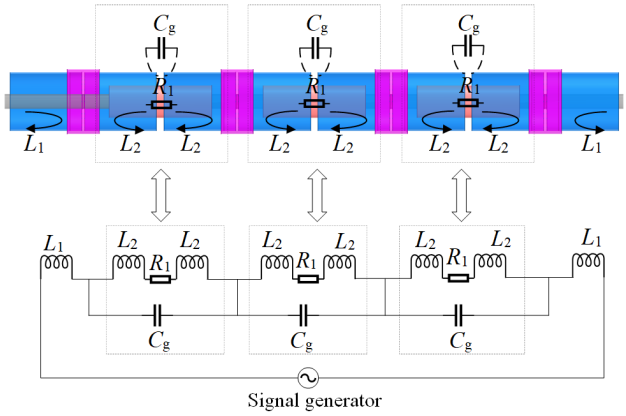

FIGURE 4. Equivalent circuit of the ferrite-EBG choke structures.

B. OPERATING PRINCIPLE

The operating principle of the ferrite-EBG composited choke structures can be explained by the equivalent resonating circuit shown in Fig. 4. The tubes of the external sides of the side elements are equivalent to inductances L_1 due to the transmission line theory. The tubes with beads are equivalent to resistance R_1 and inductance L_2 that is far greater than L_1 due to the beads. The gaps between two EBG elements are equivalent to capacitances C_g. This equivalent resonating circuit acts as a band-stop filter to suppress the parasitic currents. The values of the resistor R_1, inductor L_1, L_2 and capacitor C_g are 10 Ω, 2 nH, 31 nH and 9 pF respectively. Results of $|S_{21}|$ of the HFSS simulation and the equivalent circuit are shown in Fig. 5. The result of the circuit simulation is generally follow the trends of that in HFSS full-wave simulation. Some discrepancies occurs because the equivalent inductance, capacitance and resistance of the proposed choke structures are changed with the frequency, while in the circuit the values are stable that cannot simulate the changing characteristics. But the similar trends of the two curves in Fig. 5 indicate that the equivalent circuit can explain the operating principle of the proposed choke structures and give us some guidance in designing the structures.

III. MEASURING DEVICE

The quantitative measurement of the choke structures is difficult, because the choke structures are the part of the antenna system and the measurement is an open space problem. To turn the open space problem to a closed one, a measuring setup designed in a transmission line model is devised. As the direction of the currents flowing on the feeding cables are the same as that of the currents on the inner conductor of the measuring device, the choking effects of the proposed structures can be characterized by the $|S_{21}|$ parameter of the measuring device.

The device is designed in a transmission line model, similar to a coaxial line, which is composed of an inner conductor, outer conductors and two ports with impedance transformer circuits. The diagram of the design details is shown

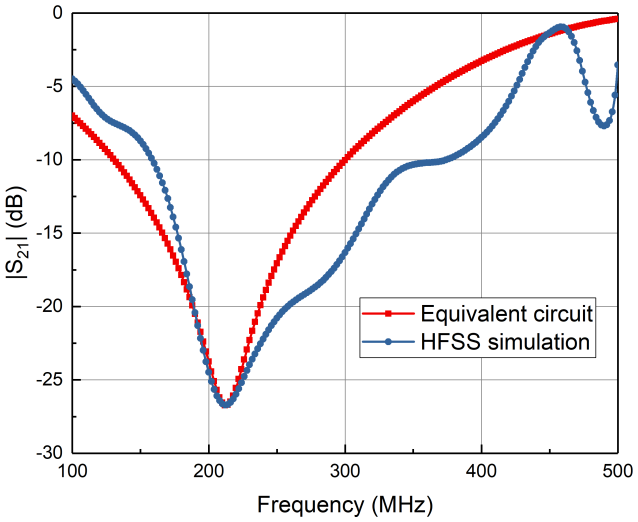

FIGURE 5. $|S_{21}|$ results of HFSS simulation and equivalent circuit.

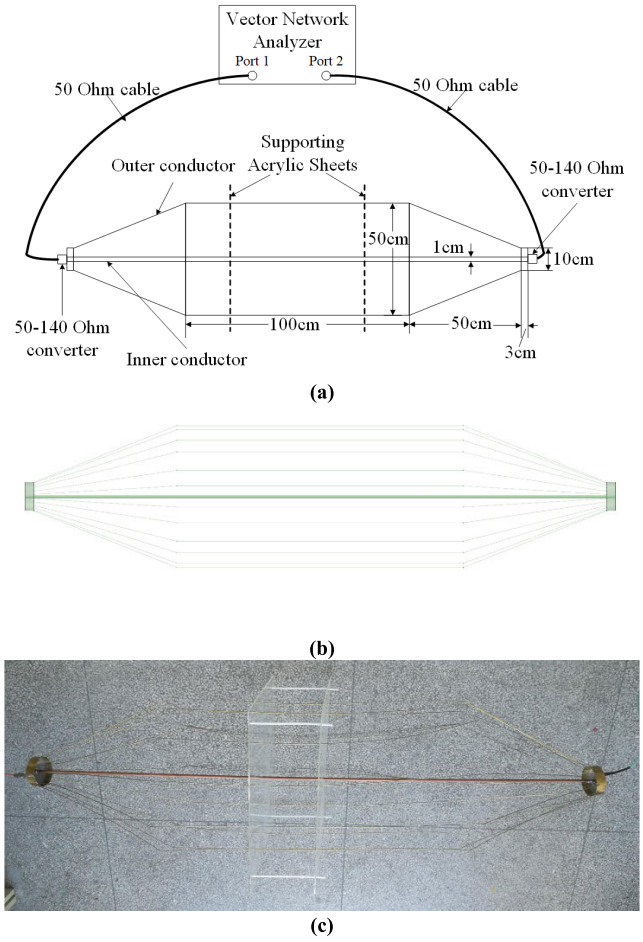

FIGURE 6. Measuring device. (a) The diagram of the design details and the connection. (b) The simulated model in HFSS. (C) The practical model.

in Fig. 6 (a). The simulated model and practical model are shown in Fig. 6 (b) and Fig. 6 (c) respectively.

The measuring device is designed in a fusiform shape, to have enough volume to accommodate the choke structures

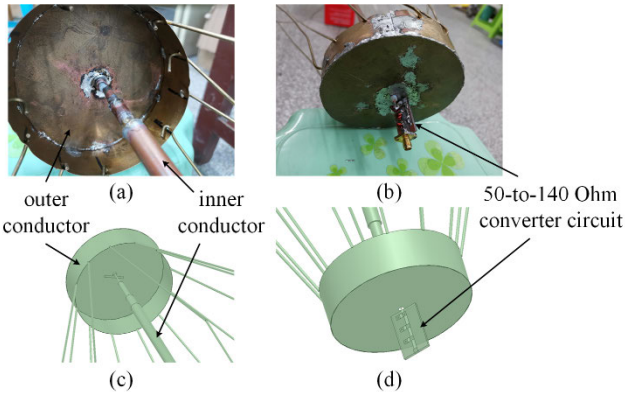

FIGURE 7. The details of the feeding ports of the measuring setup: (a) and (b) are the inner and the outer sections of the practical measuring model setup respectively, (c) and (d) are the simulated model of the inner and the outer sections of the measuring setup in HFSS software respectively.

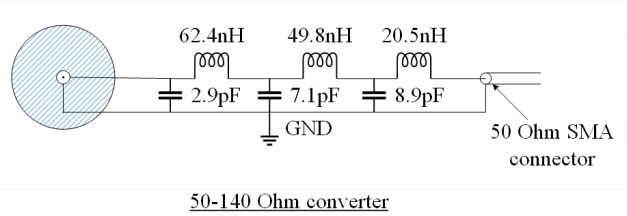

FIGURE 8. Specific circuit and values of capacitors and inductors of the 50-to-140 Ohm converter.

in the middle section of the measuring setup, and to keep enough distance between the choke structures and the outer conductor of the measuring setup, aiming to eliminate the impacts of reflecting waves from the outer metal on the operation of the choke structures. The inner conductor simulates the outer metal wrap of the coaxial feeding lines of the antenna. The inner conductor of the measuring setup gradually gets thin to its two ends, and connects to the signal paths of the 50-to140 Ohm converter circuits nearby, as shown in Fig. 7. The specific circuit and values of the elements are shown in Fig. 8. The simulated $|S_{11}|$ of the converter is shown in Fig. 9.

The choking performance of the ferrite-EBG choke structures can be measured with the measurement device. When no choke structures are added to the inner conductor, the amplitude of the transmission coefficient ($|S_{21}|$) is close to 0 dB, and the amplitude of the reflection coefficient ($|S_{11}|$) is below -10 dB in the operating frequency band at the same time, showing that current can flow freely on the inner conductor, i.e. the measuring model is an effective transmission line model. When choke structures are added to the inner conductor, the $|S_{21}|$ is below -10 dB in the operating frequency band, showing that current cannot flow on the inner conductor, proving the choking performance of the choke structures.

The simulated and measured results of the measuring device are shown in Fig. 10. Fig. 10 (a) and Fig. 10 (b) show the measured band range of $|S_{11}| < -10$ dB and

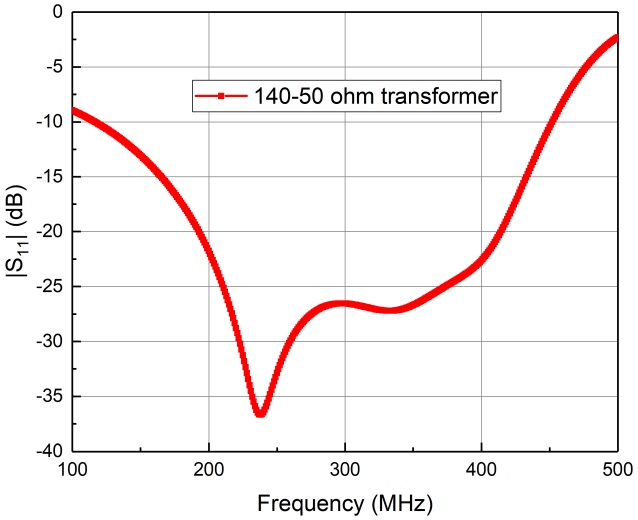

FIGURE 9. $|S_{11}|$ result of the 50-to-140 Ohm converter.

of $|S_{21}| < -1.5$dB are 131-455 MHz and 130-465 MHz respectively. $|S_{11}| < -10$ dB indicates that the model is a good transmission line model. Meanwhile, $|S_{21}|$ near 0 dB indicates that the model is of less loss and is a good transmission line model. Although the correlation between two curves in Fig. 10 (a) is not good, in practical projects, the frequency region of $|S_{11}| < -10$ dB is of our interest, and can be usually represented in VSWR < 2:1 that the discrepancy between the simulated and measured VSWR curves is relatively slight and is acceptable. In the frequency region from 131 to 455 MHz, measured $|S_{11}| < -10$ dB (shown in Fig. 10 (a)) and VSWR < 2:1 (shown in Fig. 10 (c)), showing this measuring setup is a relatively good transmission line model within this band range and can be used to test the performance of the choke structures.

IV. PERFORMANCE AND INVESTIGATION

A. PERFORMANCE COMPARISON AMONG FERRITE-EBG, EBG AND BEADS

To investigate the merits of the ferrite-EBG choke structures that combined both advantages of EBG structures and beads, the performance of the proposed choke structures with EBG structures and beads are compared. The lengths of the three structures are shown in Fig. 11. The other dimensions of the EBG structures are the same as the ferrite-EBG structures except the variable g_2, the gap between the EBG elements, which is changed from 5 mm to 0.2 mm to make it possible to compare the choke performance in the same frequency bands. Both the inner and outer diameters of the beads are the same as the ferrite-EBG choke structures.

The length of the bead with 700 mm is selected for the same reason of the variable g_2.

Fig. 12 shows the simulated $|S_{21}|$ curves of the three structures. The choking bandwidth ($|S_{21}|$ <-10 dB) of ferrite-EBG, EBG and beads are 220 MHz (from 180 to 400 MHz), 65 MHz (from 375 to 440 MHz), and 300 MHz (from 200 to 500 MHz) respectively. The ferrite-EBG structures has a much wider band than the EBG structures, and achieve

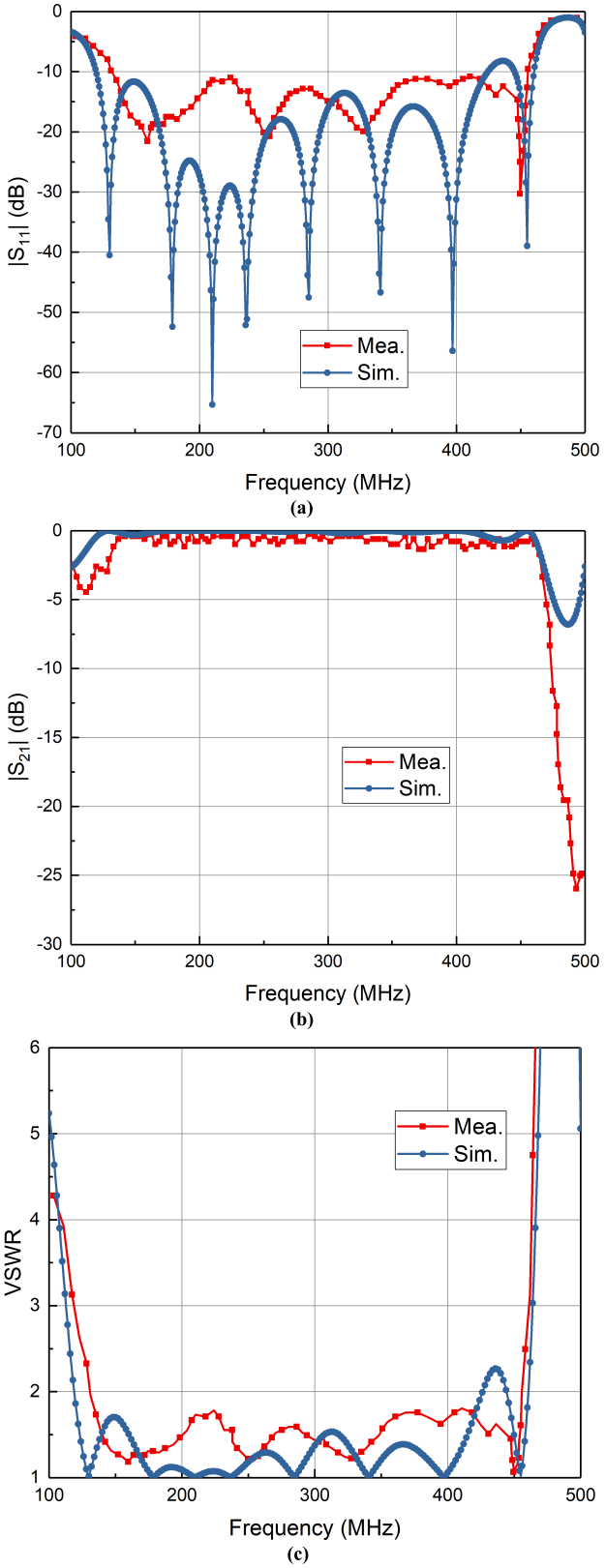

FIGURE 10. The simulated and measured results of the measuring device. (a) $|S_{11}|$, (b) $|S_{21}|$, and (c) VSWR.

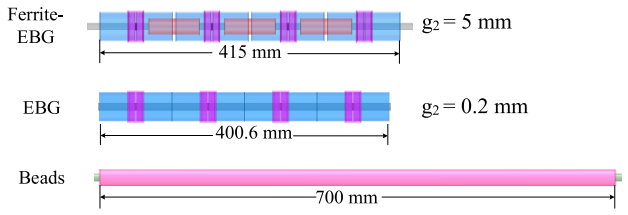

FIGURE 11. The dimensions of the ferrite-EBG, EBG, and beads.

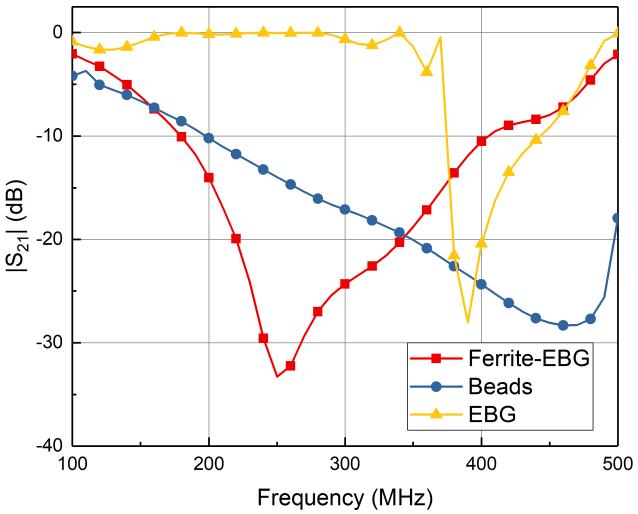

FIGURE 12. The simulated $|S_{21}|$ of ferrite-EBG, EBG, and beads.

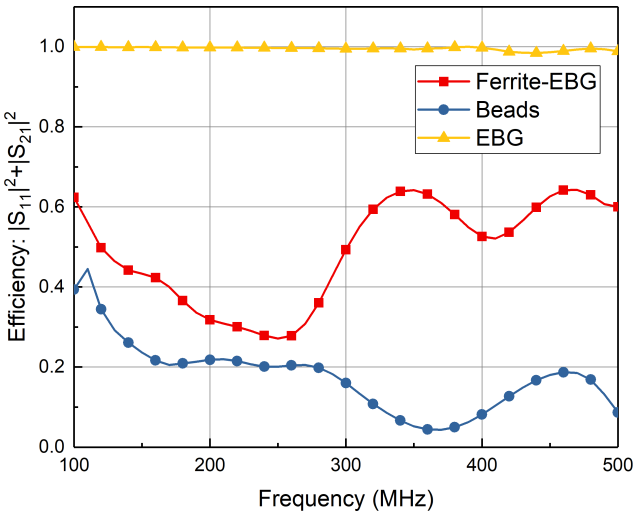

FIGURE 13. The simulated efficiency of ferrite-EBG, EBG, and beads.

two-thirds the bandwidth of beads. The efficiency of the three structures are shown in Fig. 13. The efficiency of the ferrite-EBG structures is between 0.3 and 0.6, higher than that of beads at every frequency point. The efficiency of EBG is almost close to one, showing that pure metal structures has little energy loss. With more than three times the bandwidth of the ferrite-EBG choke structures against the EBG structures, some loss in efficiency is acceptable. Therefore, the ferrite-EBG choke structures are chosen.

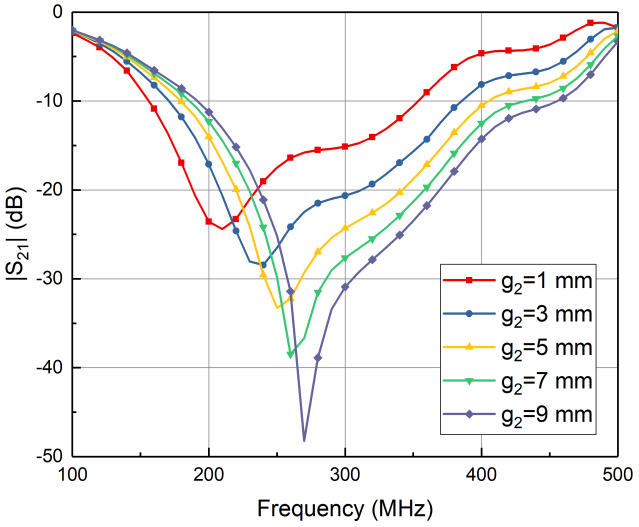

FIGURE 14. Simulated $|S_{21}|$, influence of the gap between the EBG elements (g_2) on choking bandwidth, with other variables unchanged.

B. PARAMETER ANALYSIS

This section presents the parameter analysis of four key variables of the ferrite-EBG structures, to show the influences of variables on the choke performance.

The parameters that influence the choke performance in essence influence the equivalent inductance, capacitance and resistance of the choke structures shown in Fig. 4.

The equivalent inductance is related to the lengths and the diameters of both the metal tubes and the ferrite beads. So the length h_5 and the radius r_7 of the metal tube are of our interest. The inner and outer radius of the ferrite beads are out of consideration because the beads provided by the manufacturer only have less choices in size. So only the length h_4 of the beads which can be changed by stacking different numbers of the beads is of our interest.

The equivalent capacitance is changed with the opposite area of the capacitor plates and the gap between the two plates, which in this design are composed of the opposite area of the metal tubes and the gap between the two tubes. The opposite area of the metal tubes relates to the thickness and the radius r_7 of the metal tubes. Considering the opposite area is relatively small, the thickness is not studied. The gap g1 between two tubes strongly influence the equivalent capacitance, so this parameter is in our consideration.

The equivalent resistance is mainly caused by the ohmic dissipation of the ferrite beads, and the bigger the size of the beads, the bigger the ohmic loss. The radius of the beads is out of consideration explained as before, so the length h_4 of the beads is the important influencing factor.

In summary, the length of the metal tube h_5, the radius of the metal tube r_7, the gap between two tube g_1 and the length of the beads h_4 are four important parameters for us to study the performance of the proposed choke structures.

Fig. 14 shows that the frequency point at the minima of $|S_{21}|$ shifts from 272 MHz to 210 MHz, and the choking band ($|S_{21}| < -10$ dB) changes from (193 to 456 MHz) to

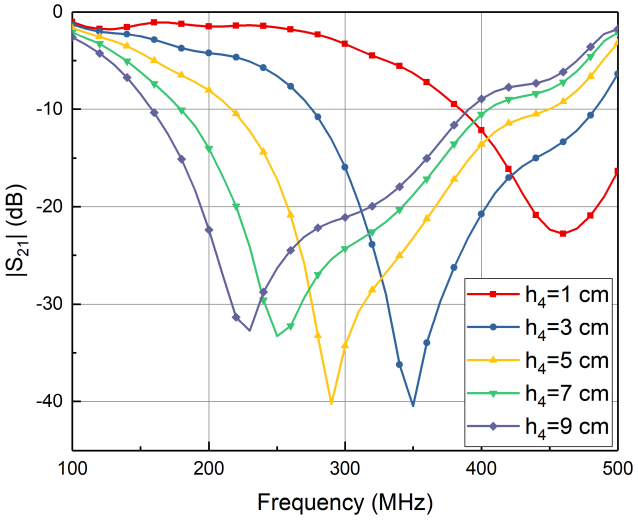

FIGURE 15. Simulated $|S_{21}|$, influence of the length of the bead element (h_4) on choking bandwidth, with other variables unchanged.

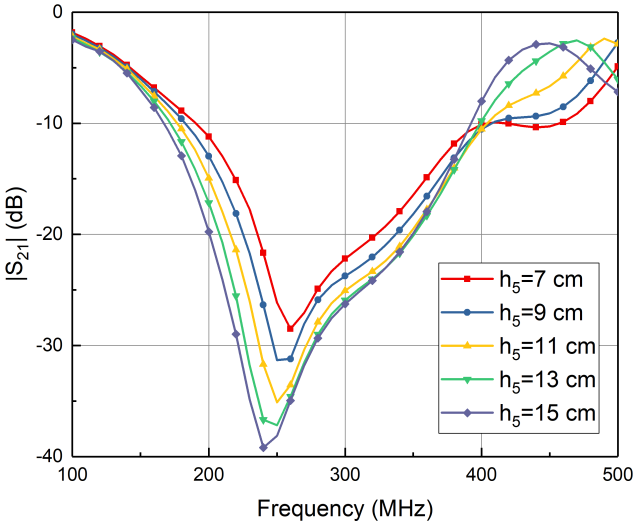

FIGURE 16. Simulated $|S_{21}|$, influence of the length of the EBG element (h_5) on choking bandwidth, with other variables unchanged.

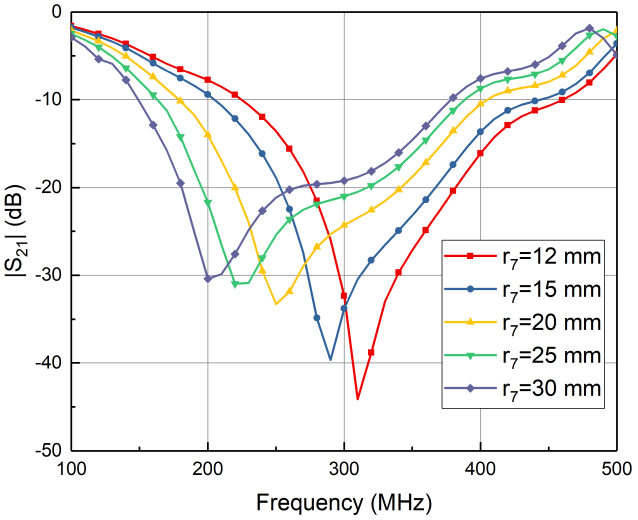

FIGURE 17. Simulated $|S_{21}|$, influence of the radius of the EBG element (r_7) on choking bandwidth, with other variables unchanged.

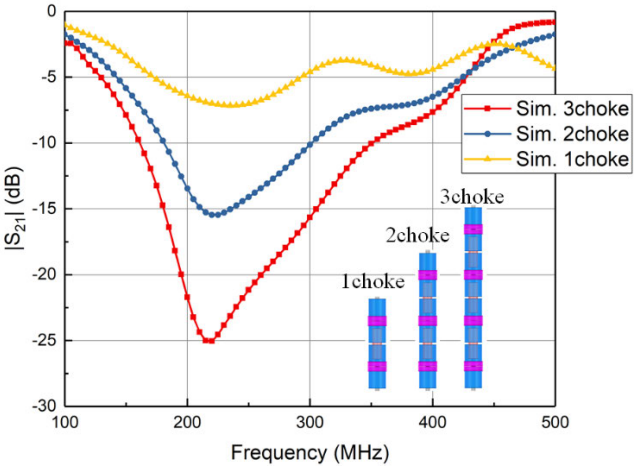

FIGURE 18. Simulated $|S_{21}|$ of different numbers of ferrite-EBG structures.

(158 to 355 MHz), with the gap between EBG elements (g_2) narrowing and other variables unchanged. This can be explained that the narrower the gap between the EBG elements, the greater the capacitance C_g (shown in Fig. 4) between two EBG elements, which will increase the mutual effect of two adjacent EBG elements and make the resonating frequency shift to the lower frequency region. The value of variable g_2 is selected based on the needed operating frequency band.

Fig. 15 shows the influence of the length of the bead (h_4) on the choking performance. The deepest point at the $|S_{21}|$ curve moves from 348 MHz to 230 MHz, and the choking band ($|S_{21}| < -10$ dB) changes from (275 to 484 MHz) to (159 to 390 MHz), with the h_4 increasing from 3 cm to 9 cm and other variables unchanged. This can be interpreted as the longer the bead, the greater the inductance L_2 (shown in Fig. 4) involved in the resonating circuit, which resulting in the lower resonating frequency.

Fig. 16 shows the resonating frequency point slightly moves from 260 to 240 MHz with the length of the EBG structures lengthening from 7 to 15 cm, which shows that the increment of the length of the EBG structures (h_5) brings relatively slight effect on the resonating frequency, and that the longer length bring a larger inductance L_1 and L_2 in the equivalent resonating circuit.

Fig. 17 shows the concave vertex of the $|S_{21}|$ curve moves from 310 to 200 MHz, and the choke bandwidth shifts from (226 to 458 MHz) to (149 to 377 MHz), with the radius of the EBG element (r_7) widening from 12 to 30 mm and other variables unchanged. This is due to the capacitance C_g (shown in Fig. 4) getting greater with the facing area of two adjacent EBG elements increasing, and the inductance L_1 and L_2 (shown in Fig. 4) getting greater with the volume of the EBG element increasing. So the resonating frequency move

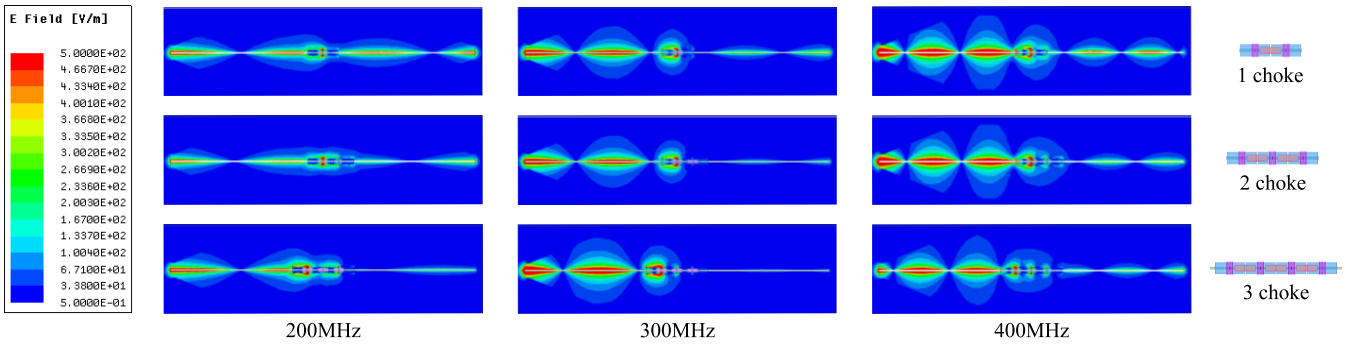

FIGURE 19. The electric fields distribution of different numbers of ferrite-EBG structures at 200, 300, and 400MHz.

to the lower region. The value of the variable r_7 is chosen based on both the choking performance and the volume.

The results of the parameter analysis show that the choking bandwidth gets wider with longer EBG, shifts to the lower bandwidth with thicker EBG, tighter EBG, and longer beads.

Considering the overall volume and the choking performance, we set $g_2 = 5$ mm, $h_4 = 7$ cm, $h_5 = 10$ cm, and $r_7 = 20$ mm.

C. THE NUMBER OF THE FERRITE-EBG STRUCTURES

The influence of the number of the ferrite-EBG structures on the choking performance is studied. Ferrite-EBG structures with one, two, and three is simulated. The $|S_{21}|$ curves of the three models are shown in Fig. 18, the choking bandwidth ($|S_{21}| < -10$ dB) of the three structures is (0 MHz), (180-300 MHz), and (160-355 MHz) respectively. So ferrite-EBG structures with three are chosen in terms of the choking performance and the volume. More elements have better choking performance, while the volume is considered as small as possible.

The electric fields distribution at 200, 300, and 400 MHz of the three models are shown in Fig. 19. For ferrite-EBG structures with three, the electric fields distribution near the inner conductor at 200, 300, and 400 MHz, is weaken when across the three choke, which turns from red to blue. For one choke, the electric field is not blocked at 200 and 400 MHz. For two choke, the electric field is not blocked at 400 MHz. So ferrite-EBG choke structures with three is enough for choking at the desired frequency region. Weighing the choke performance and the overall size, three is selected.

V. PROTOTYPE AND THE RESULTS

The prototype of the fabricated ferrite-EBG choke structures is shown in Fig. 20. The simulated and measured $|S_{21}|$ is shown in Fig. 21, with the simulated choking bands 160-350 MHz, and the measured choking bands 181-343 MHz.

The discrepancies between the simulated and measured results may be caused by three reasons.

First and the most important reason is that the inductance values of the inductors used in the 50-to-140 ohm transformer

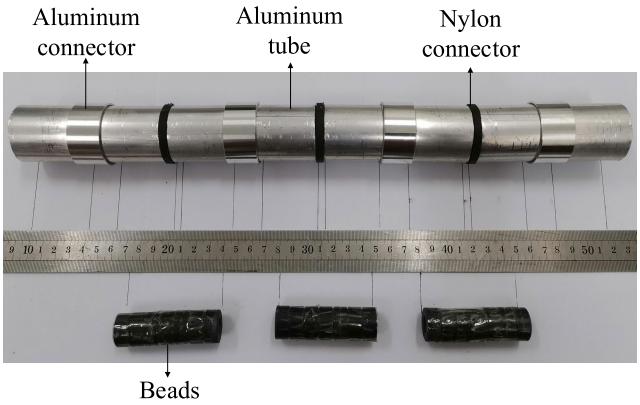

FIGURE 20. Prototype of the fabricated ferrite-EBG choke structures.

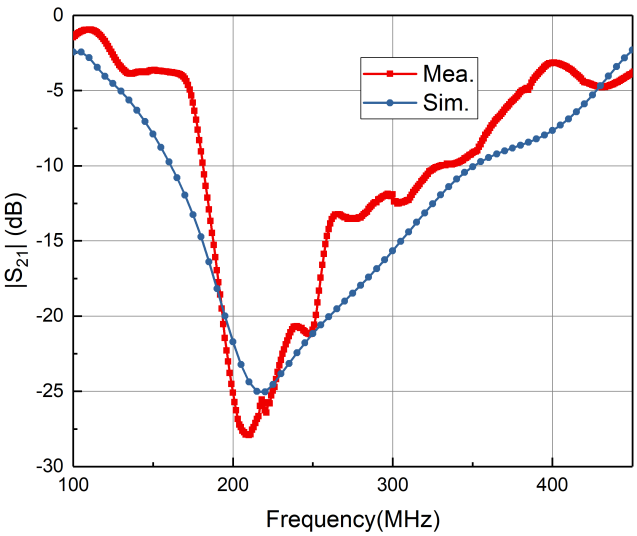

FIGURE 21. The simulated and measured $|S_{21}|$ of the ferrite-EBG choke structures.

circuit change with frequency, making the circuit not perform identically as its simulation. The inductance values of the inductors are relatively small at lower frequency and are relatively big at higher frequency, for example, an inductor is 62 nH at 120 MHz and 93 nH at 500 MHz.

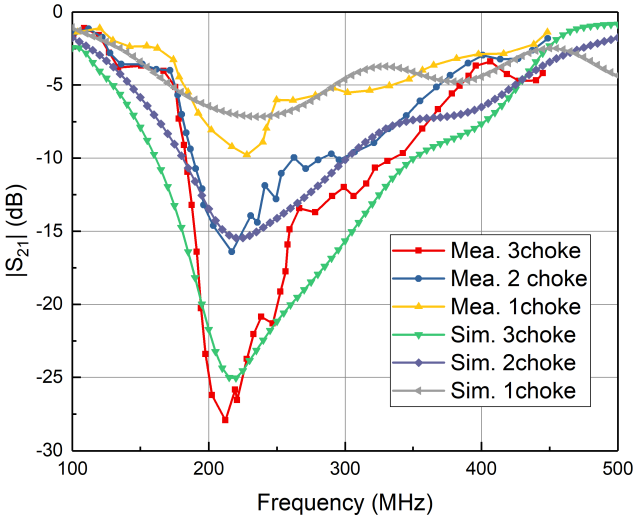

FIGURE 22. The simulated and measured $|S_{21}|$ of different numbers of the ferrite-EBG choke structures.

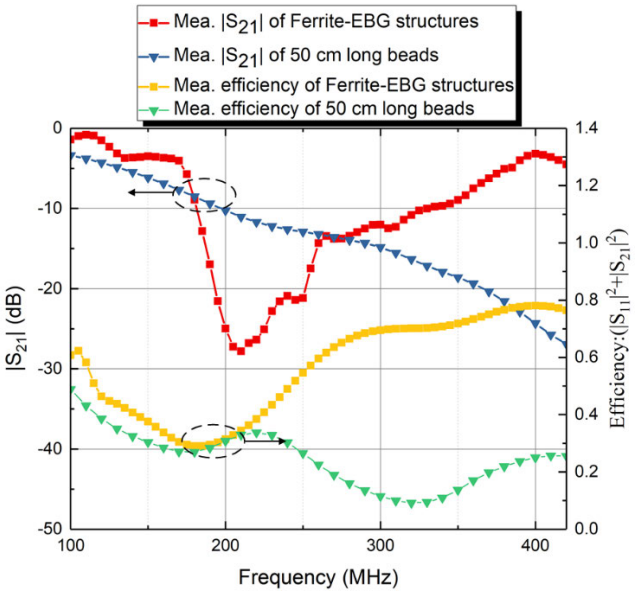

FIGURE 23. The measured efficiency and $|S_{21}|$ of the three ferrite-EBG choke structures and 50 cm long beads.

The second reason is that the actual values of the relative permeability and the magnetic loss tangent at every frequency point of the ferrite beads used in the choke structures are hard to precisely measured, and the values of the relative permeability will decrease and the magnetic loss tangent will increase with the increasement of the frequency which will degrade the choke performance of the proposed choke structures. In the simulated model we set the relative permeability value as 16 and the magnetic loss tangent as 0.512 which are given by the bead manufacturer of Beijing Seven Star Flight Electronic CO., LTD.

Last is the manufacturing errors. That the precision of the manual processing is limited.

The tendencies of the two curves are basically similar that indicates the experiment well validates the simulation.

TABLE 3. The comparison of this work with references.

Work	overall size	operating band (S21<-10 dB)	advantages	disadvantages
[1]	$0.62\lambda_L \times 0.009\ \lambda_L \times 0.009\ \lambda_L$	260-420 MHz (47.1%)	dielectric-loaded choke for miniaturization	relatively narrow band
[2]	$0.098\ \lambda_0 \times 0.05\ \lambda_0 \times 0.05\ \lambda_0$	585 MHz (single frequency point)	left-handed material for miniaturization	operating at only single frequency point
[9]	$0.29\ \lambda_L \times 0.083\ \lambda_L \times 0.083\ \lambda_L$	250-400 MHz (46.2%)	bringing in inductors and capacitors for miniaturization	inductors and capacitors may not bear the big power, relatively narrow band
This work	$0.25\ \lambda_L \times 0.024\ \lambda_L \times 0.024\ \lambda_L$	160-350 MHz (74.5%)	wideband, miniaturized, simple manufacturing	no

Fig. 22 shows the measured $|S_{21}|$ of different numbers of the ferrite-EBG choke structures. The ferrite-EBG composited choke structures with three is of the widest bandwidth which satisfy our expectance.

Fig. 23 shows the measured efficiency and $|S_{21}|$ of the ferrite-EBG composited choke structures versus that of the 50 cm long beads. With the choke performance of the proposed and the 50 cm long beads comparable, the efficiency of the proposed structures is higher at most frequency region than that of the beads.

Table 3 shows the comparison of this work with references. That our work is of relatively small size and wideband band.

VI. CONCLUSION

This paper proposes miniaturized ferrite-EBG composited choke structures, which combine the wideband choke performance of beads and the high efficiency of EBG structures. This design provides a compromise choice between choke bandwidth and efficiency. If considering the wideband choke structures, beads are the best. If considering the high-efficiency choke structures, EBG structures are the best. If considering relatively wideband and high efficiency simultaneously, the proposed design can be a candidate. We will apply these structures to the 225-400 MHz antenna to realize a miniaturized antenna in the future work.

REFERENCES

[1] A. R. Guraliuc, A. A. Serra, P. Nepa, and G. Manara, "Parasitic current reduction on electrically long coaxial cables feeding dipoles of a collinear array," *IEEE Trans. Antennas Propag.*, vol. 59, no. 11, pp. 4318–4321, Nov. 2011.

[2] T. Fukushima, N. Michishita, H. Morishita, and N. Fujimoto, "Coaxially fed monopole antenna with choke structure using left-handed transmission line," *IEEE Trans. Antennas Propag.*, vol. 65, no. 12, pp. 6856–6863, Dec. 2017.

[3] Y.-C. Tseng, H.-L. Ting, and T.-L. Wu, "A quadruplet-resonator-based ferrite-free choke for suppressing noise currents on cable shielding," *IEEE Trans. Microw. Theory Techn.*, vol. 64, no. 1, pp. 86–95, Jan. 2016.

[4] R. Qiu, F. Zhu, H. Zeng, X. Li, and J. Li, "Suppression of cable sheath current using ferrite magnetic rings," *IEEE Trans. Electromagn. Compat.*, vol. 60, no. 1, pp. 140–148, Feb. 2018.
[5] M. A. Elmansouri, J. B. Bargeron, and D. S. Filipovic, "Simply-fed four-arm spiral-helix antenna," *IEEE Trans. Antennas Propag.*, vol. 62, no. 9, pp. 4864–4868, Sep. 2014.
[6] T. Fukasawa, N. Yoneda, and H. Miyashita, "Investigation on current reduction effects of baluns for measurement of a small antenna," *IEEE Trans. Antennas Propag.*, vol. 67, no. 7, pp. 4323–4329, Jul. 2019.
[7] H. Luyen, S. C. Hagness, and N. Behdad, "Reduced-diameter designs of coax-fed microwave ablation antennas equipped with baluns," *IEEE Antennas Wireless Propag. Lett.*, vol. 16, pp. 1385–1388, 2017.
[8] Y.-M. Pan, K. W. Leung, and K. Lu, "Compact quasi-isotropic dielectric resonator antenna with small ground plane," *IEEE Trans. Antennas Propag.*, vol. 62, no. 2, pp. 577–585, Feb. 2014.
[9] X. Yang, B. Sun, L. Sun, J. Guo, and Y. Zou, "Broadband and miniaturized structure loaded with lumped capacitors for parasitic current reduction," *IEEE Antennas Wireless Propag. Lett.*, vol. 11, pp. 1010–1013, 2012.
[10] Y.-S. Wang, J.-C. Lu, and S.-J. Chung, "A miniaturized ground edge current Choke—Design, measurement, and applications," *IEEE Trans. Antennas Propag.*, vol. 57, no. 5, pp. 1360–1366, May 2009.
[11] H. Zong, X. Liu, X. Ma, S. Lin, L. Liu, S. Liu, and S. Fan, "Design and analysis of a coupling-fed printed dipole array antenna with high gain and omnidirectivity," *IEEE Access*, vol. 5, pp. 26501–26511, 2017.
[12] S.-W. Su and T.-C. Hong, "Radiation improvement of printed, shorted monopole antenna for USB dongle by integrating choke sleeves on the system ground," *IEEE Trans. Antennas Propag.*, vol. 59, no. 11, pp. 4383–4388, Nov. 2011.
[13] S. He and J. Xie, "A novel compact printed antenna used in TPMS or other complex and variable environments," *IEEE Trans. Antennas Propag.*, vol. 56, no. 1, pp. 24–30, Jan. 2008.
[14] H.-H. Sun, C. Ding, H. Zhu, B. Jones, and Y. J. Guo, "Suppression of cross-band scattering in multiband antenna arrays," *IEEE Trans. Antennas Propag.*, vol. 67, no. 4, pp. 2379–2389, Apr. 2019.
[15] J. Oh, K. Lee, T. Hughes, S. Forrest, and K. Sarabandi, "Flexible antenna integrated with an epitaxial lift-off solar cell array for flapping-wing robots," *IEEE Trans. Antennas Propag.*, vol. 62, no. 8, pp. 4356–4361, Aug. 2014.
[16] S. Karki, M. Sabbadini, K. Alkhalifeh, and C. Craeye, "Metallic monopole parasitic antenna with circularly polarized conical patterns," *IEEE Trans. Antennas Propag.*, vol. 67, no. 8, pp. 5243–5252, Aug. 2019.
[17] Z. Allahgholi Pour and L. Shafai, "A ring choke excited compact dual-mode circular waveguide feed for offset reflector antennas," *IEEE Trans. Antennas Propag.*, vol. 60, no. 6, pp. 3011–3015, Jun. 2012.
[18] H. Nakano, Y. Yamamoto, M. Seto, K. Hitosugi, and J. Yamauchi, "A half-moon antenna," *IEEE Trans. Antennas Propag.*, vol. 52, no. 12, pp. 3237–3244, Dec. 2004.
[19] R. Baggen, M. Martinez-Vazquez, J. Leiss, S. Holzwarth, L. S. Drioli, and P. de Maagt, "Low profile GALILEO antenna using EBG technology," *IEEE Trans. Antennas Propag.*, vol. 56, no. 3, pp. 667–674, Mar. 2008.
[20] M. K. Emara, J. Hautcoeur, G. Panther, J. S. Wight, and S. Gupta, "Surface impedance engineered low-profile dual-band grooved-dielectric choke ring for GNSS applications," *IEEE Trans. Antennas Propag.*, vol. 67, no. 3, pp. 2008–2011, Mar. 2019.
[21] D. J. Sawyer, S. Das, N. Diamanti, A. Peter Annan, and A. K. Iyer, "Choke rings for pattern shaping of a GPR dipole antenna," *IEEE Trans. Antennas Propag.*, vol. 66, no. 12, pp. 6781–6790, Dec. 2018.
[22] N. Chahat, L. R. Amaro, J. Harrell, C. Wang, P. Estabrook, and S. A. Butman, "X-band choke ring horn telecom antenna for interference mitigation on NASA's SWOT mission," *IEEE Trans. Antennas Propag.*, vol. 64, no. 6, pp. 2075–2082, Jun. 2016.
[23] F. Scire-Scappuzzo and S. N. Makarov, "A low-multipath wideband GPS antenna with cutoff or non-cutoff corrugated ground plane," *IEEE Trans. Antennas Propag.*, vol. 57, no. 1, pp. 33–46, Jan. 2009.
[24] L. I. Basilio, R. L. Chen, J. T. Williams, and D. R. Jackson, "A new planar dual-band GPS antenna designed for reduced susceptibility to low-angle multipath," *IEEE Trans. Antennas Propag.*, vol. 55, no. 8, pp. 2358–2366, Aug. 2007.
[25] R. Mrad, G. Pillonnet, F. Morel, C. Vollaire, and A. Nagari, "Predicting the impact of magnetic components used for EMI suppression on the base-band of a power amplifier," *IEEE Trans. Power Electron.*, vol. 30, no. 8, pp. 4199–4208, Aug. 2015.

DONGJIE QIN was born in Shanxi, China, in 1993. He received the B.Eng. degree from the Taiyuan University of Technology, Taiyuan, China, in 2015. He is currently pursuing the Ph.D. degree in electromagnetic field and microwave technology with Xidian University. His research interests include the miniaturization of VHF and UHF antenna and broadband antenna.

BAOHUA SUN was born in Hebei, China, in 1969. He received the B.Eng. degree in radio electronic from Hebei University, Baoding, China, in 1992, and the M.Eng. and Ph.D. degrees in electromagnetic and microwave technology from Xidian University, Xi'an, China, in 1996 and 2000, respectively. From 2000 to 2003, he was a Postdoctoral Research Associate with Amoi Corporation, Xia-men, China. In 2003, he joined the National Key Laboratory of Antennas and Microwave Technology, Xidian University, where he is currently a Professor. His current research interests include broadband and miniaturized antennas, broadband antenna arrays, nonfoster active antennas, mm-wave antennas, and RF circuits.